Electronic Supplemental Information of

The selective adsorption of tellurium in the

aluminosilicate regions of AFI- and MOR-type

microporous crystals

Tetsuya Kodaira [a], and Takuji Ikeda [b]*

[a] National Institute of Advanced Industrial Science and Technology, 1-1-1 Higashi,

Tsukuba, Ibaraki, 305-8565, Japan.

[b] National Institute of Advanced Industrial Science and Technology, 4-2-1 Nigatake,

Miyagino-ku, Sendai, 983-8551, Japan.

Corresponding Author

*Tetsuya Kodaira   E-mail: kodaira-t@aist.go.jp

1. **Origin of the mesopore and hindering of guest materials accessing the 1D nano-pore in AFI type crystals.**

Image of aggregated $AlPO_4$-5 crystals are drawn in Fig. S1. $AlPO_4$-5 has isolated 1D nano-channels arrayed parallel to **c**-axis.   Therefore, if the crystals are aggregated with random orientation, surrounding attached crystals might be the origin of closing the entrance of the channel.   When there are two closed sites for a channel, area between them becomes dead space.   Defects, contaminations, alumino-silicate regions distributed in a SAPO-5 crystal and so on are the candidates reducing the active volume of the 1D nano-channels.   In order to avoid or improve the degradation of porosity, utilization of highly dispersed $AlPO_4$-5 crystals with small size might be the answer, because the shorter channel length makes the low possibility for encountering the origins of the channel closing.

1D nano-channel of $AlPO_4$-5
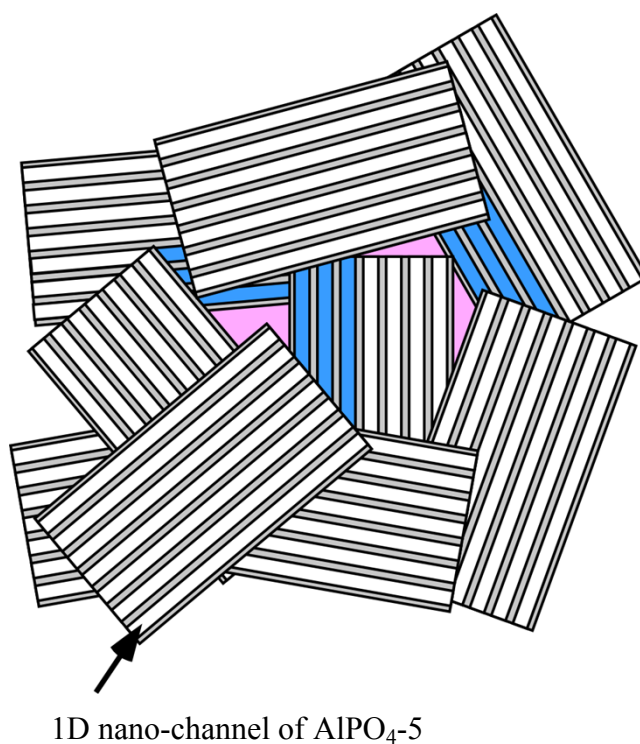
Fig. S1.   Illustration of aggregated $AlPO_4$-5 crystals.   Channels colored in blue are both side closed.   Areas shown by pink color are nonnative mesopores generated among the crystals.

2. Verification of crystallinity on MORs by ion-exchanging and calcining treatment.

NH$_4$-MOR was obtained by the ion exchange of Na-MOR soaking into NH$_4$NO$_3$ aq. solution. NH$_4$-MOR gives no difference on its widths on diffraction peaks compared with those of Na-MOR. Furthermore, H-MOR from NH$_4$-MOR by calcining at 773 K also shows no degradation on its crystallinity estimated from the diffraction peak width in Fig. S2. On the relative intensities of diffraction peaks, we can clearly see the variation of relative intensities of 110 and 020 diffraction peaks in the patterns by changing cations from Na$^+$ to H$^+$ through NH$_4^+$. This indicates the ion-exchanges are successfully taken place.
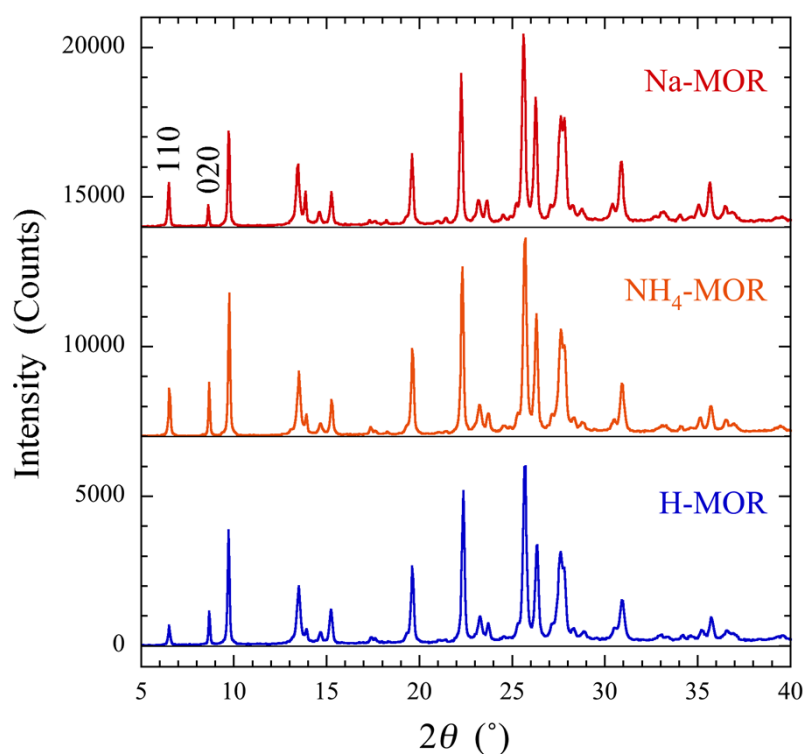
Fig. S2. Powder XRD patterns of Na-MOR, NH$_4$-MOR, and H-MOR measured by using Cu-Kα radiation.

3. Chemical analyses of Na-MOR and H-MOR.

Energy dispersive x-ray fluorescence (XRF) spectra were obtained using Bruker Quantax XFlash® 6|100, attached to the SEM apparatus. XRF spectra of Na-MOR and H-MOR are shown in Fig. S3. Derived from the XRF data, Si/Al ratios were invariant with the treatment of ion exchange from Na^+ to H^+, and Na^+ was effectively exchanged to H^+ as listed in Table S1. The chemical formula of Na-MOR determined by chemical analysis was $Na_{5.5}Al_{5.5}Si_{42.5}O_{96}$, that gives Si/Al = 7.7.
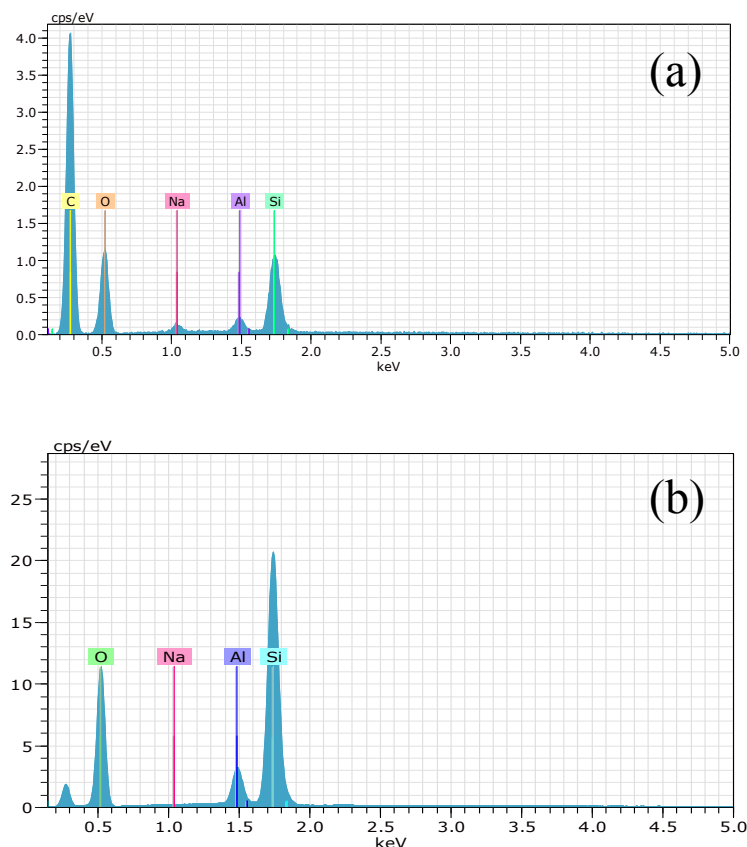
Fig. S3.   XRF spectra of (a): Na-MOR and (b): H-MOR

Table S1.   Obtained results for chemical compositions from the EDX analysis

Material	Na	Al	Si	O	(Atomic percent (%))
Na-MOR	3.33	3.79	28.51	64.37	
H-MOR	0.01	4.08	29.47	66.45	

Material	Si-to-Al atomic ratio	Na-to-Al ratio
Na-MOR	7.5	0.87
H-MOR	7.2	0.00

4.   Lists of the apparatuses and their conditions used for the analyses.

- Powder x-ray diffraction patterns

The Bragg-Brentano type goniometer (MXP-3TZ, MAC Science), equipped with a pair of solar slits with a divergence angle of 1˚ was used with Cu-Kα radiation. The patterns were measured under a condition of constant irradiation area for a sample independent of $\theta/2\theta$ angles by using variable width type divergence and scattering slits.

- Scanning electron microscope (SEM) images and chemical analysis.

SEM images were obtained by using S4800 (Hitachi).   Acceleration of the scanning electron beam was 1 kV.   Chemical formulae of Na-MOR and H-MOR were confirmed by using energy dispersive x-ray fluorescence detector Quantax XFlash® 6|100 (Bruker) attached to this SEM.

- Adsorption-desorption isotherms

Prior to the measurement, AlPO$_4$-5 was dehydrated at 473 K for 12 h using an oil rotary pump.   Porosity of AlPO$_4$-5 powder was evaluated at 77 K using Autosorb-1 (Quantachrome) with an adsorbent gas of N$_2$.   Surface area was estimated using the BET method for data points of P/P_0 = 0.008–0.025, where $1/[nP/(P_0-P)]$ was liner. Pore size distribution was obtained by using the Saito-Foley (SF) method.

- Optical absorption spectra

Diffuse reflection spectra, which are converted into absorption spectra using the Kubelka-Munk function, were obtained using Cary5000 (Varian) equipped with a handmade diffuse reflection unit.   Here we note that absorption spectra derived using the Kubelka-Munk function are comparable on their absorption intensity in case of same particle size.   Example of quantitative analysis on the absorption intensity is written in the article by Kodaira and Murakami, *J. Chem. Phys.* 2007, **127**, 094704.

- TG-DTA curves

The TG-DTA curves were measured using Thermo plus EVO II series TG8120 (Rigaku).   Samples were heated under conditions of a temperature elevation speed of 5 K/min. and a dried airflow of 50 ml/min.

5. Pore distribution analysis of AlPO$_4$-5.

Nitrogen gas adsorption isotherm of AlPO$_4$-5 shows high microporosity, as shown in Fig. 3.   The adsorption volume of nitrogen gas was monotonically increased with increasing relative pressure without a step. The BET surface area was estimated as 371 m^2·g^{-1}. The cumulative micropore volume was estimated to be 0.135 ml·g^{-1} for the pore diameter region of 0–2 nm by means of the Saito-Foley (SF) method as plotted in Fig. S4.   The micropore diameter was determined to be ca. 0.95 nm; however, it should be noted that the pore diameter tends to be overestimated in nitrogen adsorption measurement.

An ideal pore volume of AlPO$_4$-5 was calculated as follows.

Pore volume of 1D nano-channel per unit cell, $V_{u.c.}$, is $V_{u.c.} = \pi r^2 c$, where r is a radius of the channel and c is the lattice constant of a unit cell in **c**-axis direction.   The pore volume per unit cell, $V_{u.c.}$, was converted into per gram, V_g, by an equation of $V_g = V_{u.c.} N_A / M$, where N_A is Avogadro's constant and M is the molar weight of dehydrated AlPO$_4$-5, *i.e.* Al$_{12}$P$_{12}$O$_{48}$.   Practical values are $r = 0.73/2 = 0.365$ nm, $c = 0.84$ nm, $N_A = 6.03 \times 10^{23}$, $M = 1463$.
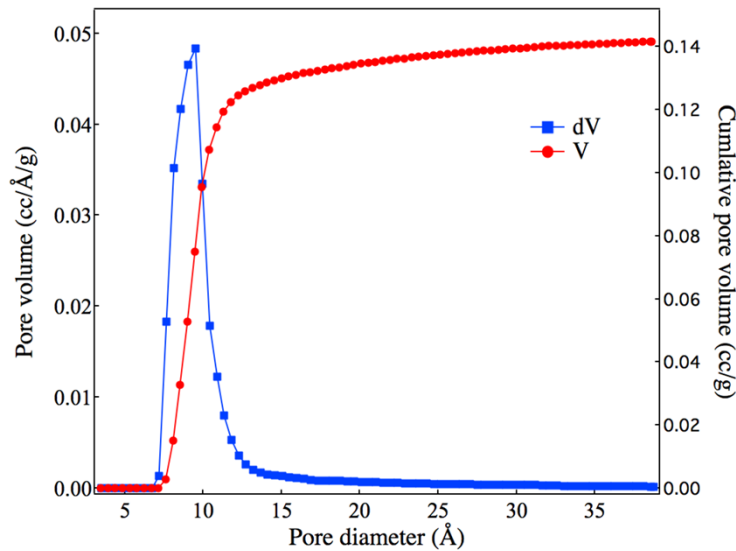
Fig. S4.   Pore size distribution curve (blue) and adsorption volume curve (red), which are derived from N$_2$ adsorption isotherm shown in Figure 3 of main text, using the SF method.

6. Determination method on the adsorbed amounts of Te atoms

From the TG curves shown in Fig. 7 A in the main text, chemical formulae of AlPO$_4$-5, H-MOR, and Na-MOR in hydrated form were determined as Al$_{12}$P$_{12}$O$_{48}$ · 18.8H$_2$O, H$_{5.5}$Al$_{5.5}$Si$_{42.5}$O$_{96}$ · 25.0H$_2$O, and Na$_{5.5}$Al$_{5.5}$Si$_{42.5}$O$_{96}$ · 22.8H$_2$O, respectively.

Moles of used micro-porous crystals (m-c), $M_{\text{m-c}}$, can be calculated from the upper chemical formulae. Moles of actually loaded Te, M_{Te}, can be derived by subtracting the weight of residual lump from that of initial lump. The ratio $M_{\text{Te}}/M_{\text{m-c}}$, N, is the number of Te atoms adsorbed in each unit-cell.

In order to compare the obtained values, N_{AlPO_4-5}, N_{H-MOR}, and N_{Na-MOR}, they have to be normalized into 1 nm in length in each 1D-nanochannels. There are one and two 1D nano-channels in AlPO$_4$-5 and mordenite that are both parallel to **c**-axis, respectively, and the channels lengths in unit cells are equal to lattice constants c of 0.84 and 0.75 nm, respectively. Therefore, for AlPO$_4$-5 and SAPO-5, the normalized number density is,

$$N_{AlPO_4-5\ or\ SAPO-5}/0.84 = 1.19 N_{AlPO_4-5\ or\ SAPO-5}, \qquad (\text{S-1})$$

and for mordenites, they are

$$N_{Na-MOR\ or\ H-MOR}/2/0.75 = 0.67 N_{Na-MOR\ or\ H-MOR}. \qquad (\text{S-2})$$

7. Models of possible isolated Te chains.

Fig. S5(a) is a Te chain with three-fold spiral (trigonal) structure extracted from trigonal Te crystal structure. The bond length between the nearest Te atoms is 0.263 nm, and the bonding angle is 110.4°. Under conserving these bond length and the bond angle of the bulk crystal, i.e. only varying the dihedral angle from 105.0° to 0° (180°), zigzag structure as illustrated in Fig. S5(b) gives the lowest atomic numbers per length in a chain. If the bonding angle can be also a variable, a strait chain (bonding angle: 180°) gives lower atomic numbers than the zigzag structure as in Fig. S5(c). Resulting, the trigonal, zigzag, and strait chains provide 5.0, 4.6, and 3.8 atoms per nm along the chains, respectively.

(a) (b) (c)
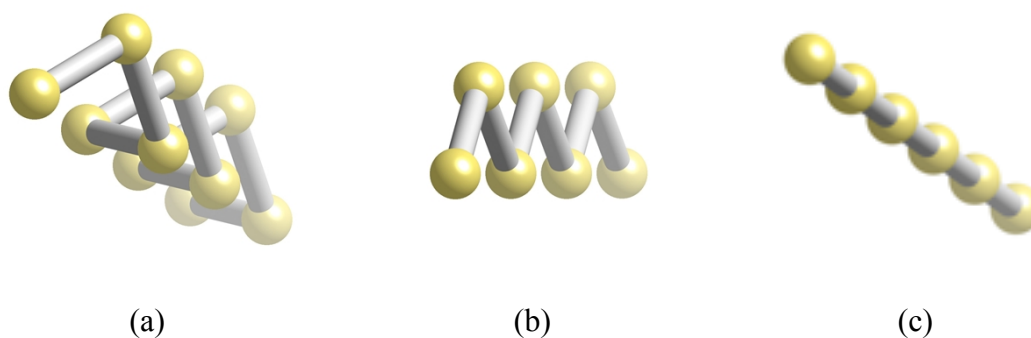
Fig. S5. (a): Trigonal, (b): zigzag, and (c): strait chain models.

8. Derivation of acid point numbers in SAPO-5

We referred experimental results in Ref. 17 listed in the references of the main article.

SAPO-5 used in the present work is Si/(Al+Si+P) = 0.046.   In the referred article, NH_3 temperature programmed desorption curve of SAPO-5 sample with Si / (Al+Si+P) = 0.045 was measured.   According to its result, this SAPO-5 has acid points of 0.4–0.45 mmol/g.   Dehydrated SAPO-5 ($AlPO_4$-5) has a molecular weight of *ca*. 1500. 1 g of SAPO-5 is $6.8×10^{-4}$ mol.   Thus, acid points per unit cell can be derived as,

$$\left(0.4–0.45×10^{-3}\right) / (6.8×10^{-4}) = 0.6–0.7 \qquad \text{(/unit cell).}$$

Because the lattice constant of **c**-axis is c = 0.84 nm, the acid points in one 1D nano-channel per 1 nm in length are derived,

$$(0.6–0.7) / 0.84 = 0.7–0.8 \qquad \text{(/channel/nm).}$$